JACS
JOURNAL OF THE AMERICAN CHEMICAL SOCIETY
Article
Cite This: J. Am. Chem. Soc. 2017, 139, 16273-16281
pubs.acs.org/JACS

Mitochondria Alkylation and Cellular Trafficking Mapped with a Lipophilic BODIPY−Acrolein Fluorogenic Probe

Richard Lincoln, Lana E. Greene, Wenzhou Zhang, Sheena Louisia, and Gonzalo Cosa*

Department of Chemistry and Center for Self-Assembled Chemical Structures (CSACS-CRMAA), McGill University, 801 Sherbrooke Street West, Montreal, Quebec H3A 0B8, Canada

Supporting Information

ABSTRACT: Protein and DNA alkylation by endogenously produced electrophiles is associated with the pathogenesis of neurodegenerative diseases, to epigenetic alterations and to cell signaling and redox regulation. With the goal of visualizing, in real-time, the spatiotemporal response of the cell milieu to electrophiles, we have designed a fluorogenic BODIPY−acrolein probe, **AcroB**, that undergoes a >350-fold fluorescence intensity enhancement concomitant with protein adduct formation. **AcroB** enables a direct quantification of single post-translational modifications occurring on cellular proteins via recording fluorescence bursts in live-cell imaging studies. In combination with super-resolution imaging, protein alkylation events may be registered and individually counted, yielding a map of protein−electrophile reactions within the cell lipid milieu. Alkylation is predominantly observed within mitochondria, a source, yet not a sink, of **AcroB** adducts, illustrating that a mitochondrial constitutive excretion mechanism ensures rapid disposal of compromised proteins. Sorting within the Golgi apparatus and trafficking along microtubules and through the cell endo- and exocytic pathways can be next visualized via live-cell imaging. Our results offer a direct visualization of cellular response to a noncanonical acrolein warhead. We envision **AcroB** will enable new approaches for diagnosis of pathologies associated with defective cellular trafficking. **AcroB** may help elucidate key aspects of mitochondria electrophile adduct excretion and cell endocytic and exocytic pathways. Conceptually, **AcroB** provides a new paradigm on fluorescence microscopy studies where chemical perturbation is achieved and simultaneously reported by the probe.

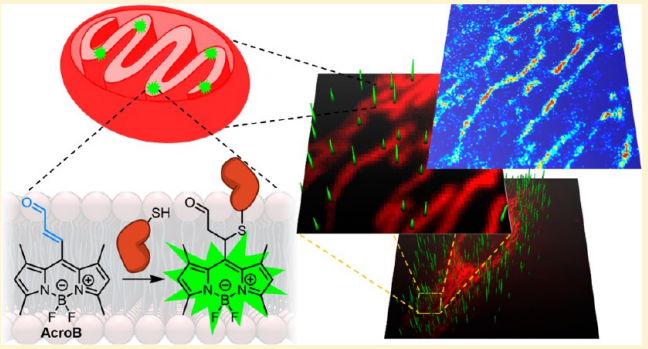

INTRODUCTION

Lipid-derived electrophiles (LDE) are highly reactive species generated within cellular membranes as byproducts of enzymatic oxidation of polyunsaturated fatty acids or their catalytic autoxidation under oxidative stress conditions.[1−4] Five of the most abundantly studied LDEs include 4-hydroxy-2-nonenal (4-HNE), 4-oxo-2-nonenal, acrolein, 2-*trans*-hexadecenal, and 15-deoxy-Δ12,14-prostaglandin J2 (Figure 1A). The former four share the α,β-unsaturated aldehyde (enal) warhead and, with the exception of acrolein, a residual aliphatic tail from the lipid source. LDEs undergo Michael addition reactions leading to cellular DNA and protein alkylation. The latter typically involves nucleophilic attack by cysteine residues but also, and to a lesser extent, other nucleophilic amino acids including histidine and lysine.[5]

Implicated in cellular toxicity and the pathogenesis of neurodegenerative diseases[2,3] and atherosclerosis,[6] among others, LDEs may also serve beneficial physiological roles as messengers to modulate cellular responses to electrophile stress.[7,8] They may be associated with epigenetic changes[9] and are, as of recently, being exploited in novel therapeutic drugs based on electrophile reaction.[10]

The ubiquitous nature of LDEs and the plethora of biological outcomes associated with their electrophilic chemical reactions have jointly sparked a wide interest in monitoring their presence and the nature of the products formed. A number of proteomic studies have characterized the reaction products and off-targets associated with physiological (1 μM or less)[2,3,11] concentrations of LDEs.[5,12]

Inspired by the chemistry of LDEs and with the goal of visualizing in real-time the spatiotemporal response of the cell milieu to electrophiles, we have developed a new approach that involves a noncanonical acrolein warhead and blends elements of fluorescence imaging and super-resolution imaging with probe design. Our strategy ultimately provides a spatiotemporal chart that reflects where electrophile−protein adducts are formed, how long they reside, where they accumulate, how they are sorted, which key organelles are involved in their processing, and what are the trafficking dynamics.

By using the enal warhead as a rotamer-based quencher of the fluorescence of a lipophilic BODIPY fluorophore,[13,14] we have constructed a fluorogenic probe (**AcroB**, Figure 1B) that

Received: August 13, 2017
Published: October 4, 2017

DOI: 10.1021/jacs.7b08615
J. Am. Chem. Soc. 2017, 139, 16273−16281

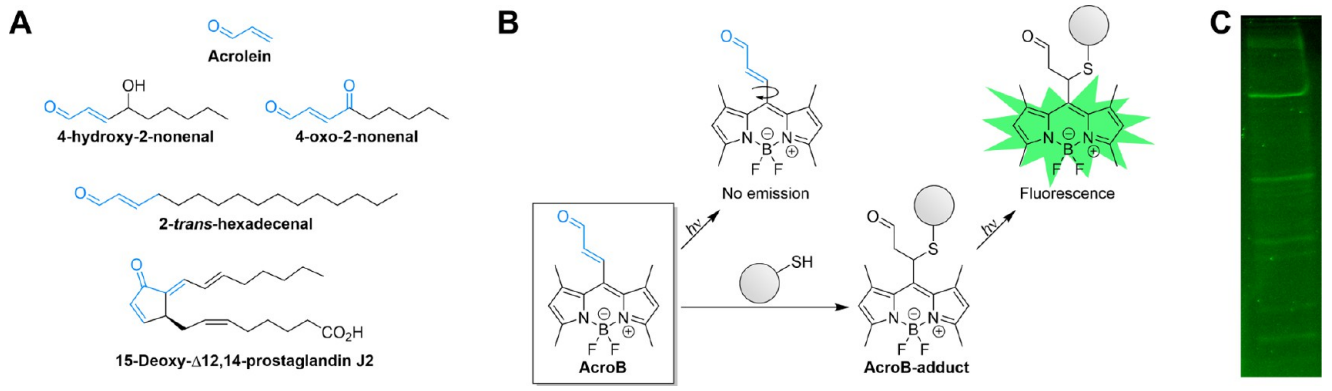

Figure 1. (A) Molecular structures of LDEs with the reactive moiety highlighted in blue. (B) Mechanism of action of **AcroB**. (C) SDS-PAGE of **AcroB** protein adducts from HeLa cell fractions.

is capable of reporting—via a larger than 350-fold emission enhancement—on post-translational modifications occurring on membrane-embedded/-associated proteins. While the reactivity of **AcroB** will suffer from the proximity of the BODIPY dye, which sterically hinders the reaction center and may influence noncovalent interactions/affinity with protein targets, the probe illustrates general concepts of the spatiotemporal controlled reactivity of lipophilic electrophiles at the cellular level.

Working with two cell lines, HeLa and MRC5, the high off/on sensitivity of **AcroB** enabled real-time visualization and quantification (via single-molecule fluorescence burst counting) of protein post-translational modifications (PTM) occurring in live cells. **AcroB** further reported on the accumulation, sorting, and recycling of newly formed LDE adducts, illustrating their trafficking dynamics through the cell endocytic and exocytic pathways. Intriguingly, our work shows that mitochondria are the predominant site for LDE adduct formation, yet rapid evacuation of newly formed adducts was recorded, illuminating what we believe is a mitochondrial protection pathway. Mitochondria are thus a source yet not a sink of **AcroB** adducts.

Our results offer a direct visualization of cellular response to a noncanonical lipophilic electrophile and provide an example where chemical perturbation on the system is actively performed and simultaneously reported by the probe.

RESULTS AND DISCUSSION

Probe Design and Characterization. In designing and preparing the fluorogenic compound **AcroB** (see also the Supporting Information), we were inspired by previous work from our group[13,14] showing that *meso*-formyl BODIPY dyes are highly reactive electrophiles that undergo emission enhancement upon nucleophilic attack. The lipophilic nature of the BODIPY core provided, we reasoned, an ideal fluorescence reporter of reactivity within the cellular lipid milieu with absorption in the visible range (λ_{max} 503 nm in acetonitrile).[15−17] The sensitivity of the BODIPY fluorescence intensity to the presence of an unsaturation at the *meso*-position[14] was in turn exploited toward reporting Michael addition reactivity. Unsaturated moieties at the *meso*-position lead to suppression of BODIPY fluorescence via excited-state conjugation of the disconnected π-systems (see Figure S1 for rationalization by density functional theory and time-dependent density functional theory calculations).[18,19] Positioning the α,β-unsaturated aldehyde moiety at the *meso*-position of the BODIPY scaffold thus rendered a nonemissive acrolein warhead. The methyl groups of the BODIPY scaffold ensure that the BODIPY and acrolein π-systems remain uncoupled, preserving the electronic nature of the enal moiety (a reduced reactivity is, however, expected to arise from steric blocking of the reaction site). This is consistent with the ^{13}C NMR of **AcroB**, which closely matches that of free acrolein with differences within 3 ppm. Specifically, we measure 191.9, 141.9, and 137.8 for the acrolein warhead of **AcroB**, and we measure 194.4, 138.4, and 137.9 ppm for free acrolein. Michael addition by a protein nucleophilic residue and concomitant destruction of the *meso*-unsaturation restored the BODIPY fluorescence (Figure 1B,C).

To establish the sensitivity and selectivity of **AcroB** reaction with nucleophiles of biological relevance and the role the environment plays in modulating **AcroB** reactivity, we conducted fluorescence versus time (up to 1 h) studies under physiological (1 μM)[2,3,11] concentrations of the fluorogenic electrophile in the presence of millimolar concentrations of amino acids at pH 7.4 (Figure S2). Within the 1 h monitoring time, fluorescent enhancement was observed with L-cysteine only, albeit weak at ca. 9-fold. L-Lysine and L-histidine, while less reactive than L-cysteine, are known targets of LDEs; however, they form Schiff base adducts that may not restore fluorescence as they preserve the *meso*-unsaturation.[14] We further observed no reaction of **AcroB** with aqueous glutathione (GSH) solutions. Addition of glutathione-S-transferase (GST), a catalyst for GSH addition to electrophiles,[3] led, however, to a ∼350-fold enhancement in intensity consistent with the formation of a fluorescent **AcroB**−glutathione adduct (λ_{max} 517 nm). Importantly, GST-catalyzed adduct formation was significantly diminished in the presence of lipid vesicles (Figure S1E). The lipophilic nature of **AcroB** was confirmed upon measuring its partition coefficient (P) by reverse-phase HPLC (see Table S1).[20,21] We obtained a log(P) value of 3.1 ± 0.2 for **AcroB**, similar to values reported for other BODIPY dyes used for membrane imaging.[22] Our results indicate that **AcroB** is located within the lipid membrane, where the BODIPY scaffold ensured sequestration from the water pool. Undesired reactions with cytosolic thiol sources, specifically GSH present in millimolar concentration, may thus be averted.

Super-resolution Mapping of AcroB Adduct Formation. In order to establish the suitability of **AcroB** toward imaging alkylation of membrane proteins in living cells, HeLa cervical cancer cells (ATCC CCL-2) on fibronectin-conditioned coverslips were treated with 10 nM, 100 nM, and 1 μM **AcroB** and imaged via fluorescence microscopy. The dye was

DOI: 10.1021/jacs.7b08615
J. Am. Chem. Soc. 2017, 139, 16273−16281

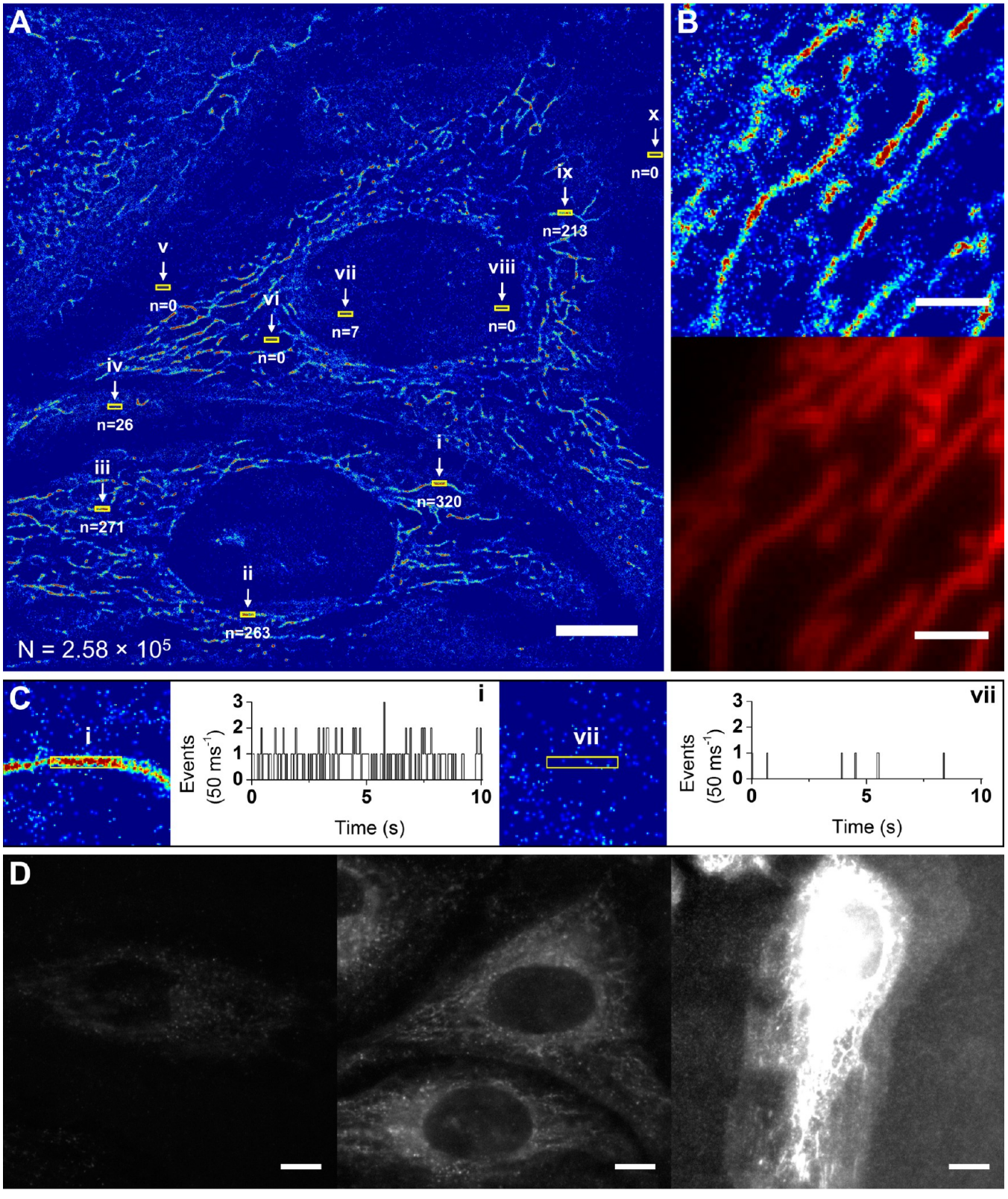

Figure 2. (A) NASCA high-resolution map of individual PTM events in a HeLa cell accumulated over 500 consecutive frames (25 s) following treatment with 100 nM **AcroB.** *N* is the total number of observed chemical events. Events were counted if their intensity was greater than 1000 photons and less than 20000 photons. *n* is the number of chemical events counted in 1.66 μm × 250 nm regions within regions of interest corresponding to mitochondria (i, ii, iii, ix), the nucleus (vii, viii), cellular regions with no apparent organelle (iv, vi), and extracellular regions (v, x) are listed. (B) Colocalization of **AcroB** adduct hot-spots (top) with MitoTracker Deep Red (bottom). (C) Event−time trajectories of **AcroB** adduct formation recorded in regions i and vii. (D) Single frames showing concentration dependence of **AcroB** adduct formation at 10 nM (left panel), 100 nM (middle panel), and 1000 nM (right panel) **AcroB**. Scale bars are 10 μm except (B) at 2 μm.

DOI: 10.1021/jacs.7b08615
J. Am. Chem. Soc. 2017, 139, 16273−16281

delivered from DMSO stock solutions such that the final concentration of DMSO was 0.33% by volume. The **AcroB** concentration selected for our studies was on par with basal levels of the well-studied LDE 4-HNE[2,3,11] and showed no toxicity to HeLa cells up to 1 week following administration (see Figure S3).

To observe formation of single fluorescent **AcroB**−protein adducts, that is, single chemical events, with sufficient signal to background ratio, the laser excitation power was set to 42 mW in our cell imaging experiments. We further utilized the evanescent beam in a total internal reflectance (TIRF) microscope setup to minimize background.

Imaging with 100 nM **AcroB** at a frequency of 20 Hz (50 ms frame) revealed the appearance of fluorescence spots over the whole cell extension. The high excitation powers employed ensured **AcroB** adduct photobleaching occurred within 50−100 ms upon formation (the burst lifetime we determined was a fraction (0.75) of a frame; see Figure S4). The formation of single nucleophile adducts of **AcroB** was thus recorded as fluorescence bursts in our experiments (Figure 2 and accompanying supplementary Video S1). Imaging was conducted in a pulse-chase scheme, monitoring live cells prior to and immediately following addition of **AcroB**. Response was immediate. Our analysis involved discarding the first 100 frames until a steady-state burst occurrence was achieved, where **AcroB**−protein adducts were generated and photobleached at a similar rate.

Recording stochastic fluorophore activation events provided rich spatial information[23−25] on the reactivity of the lipophilic electrophile, **AcroB**, at the nanoscopic level within a live cell. The mathematical localization of individual fluorescence bursts performed via nanometer accuracy by stochastic chemical reaction/activation (NASCA) microscopy[26] analysis rendered a new highly resolved image combining results from 500 frames (25 s imaging period; see Figure 2A). The spots traced a vast network resembling mitochondria. This assignment was confirmed upon colocalization imaging in the presence of MitoTracker Deep Red (Figure 2B and Video S2). Cross-section analysis of the filaments along the network revealed features ca. 130 nm in width/diameter on average.

In addition to the major localization within mitochondria, we also observed sporadic events distributed over the cell, including the nuclear region where, however, events were rare. To establish that **AcroB** reactions are not photoinduced, we inspected emission from cells far away from the illumination region, which displayed equivalent intensity outputs. Increasing **AcroB** concentration from 10 to 100 nM resulted in a proportional increase in the frequency of fluorescence bursts detected within mitochondria. At 1 μM **AcroB**, individual bursts were no longer distinguishable and the whole organelles were lit up (Figure 2D; see also the accompanying supplementary Video S3). Experiments conducted with 10 nM compound showed that the rare, sporadic fluorescence bursts are unique in time and place. They are not followed by subsequent events/clustering of events, what would be otherwise expected should blinking follow the genesis of a newly emissive compound.

AcroB localization, reaction, and ensuing fluorescence activation almost exclusively within mitochondria are consistent with the nature of many mitochondrial proteins that bear functional, electrophile-reactive, cysteine residues.[27,28] The remarkably high reactivity within mitochondria versus the rest of the cell may be additionally rationalized by the higher proportion of highly reactive thiolate anions over the less reactive conjugate acid thiols in this organelle relative to other cell compartments.[27] The pH 8 within the matrix of respiring mitochondria, combined with the pK_a values for thiols in the range of 8.5−9, renders the matrix a hot-spot for nucleophilic attack by thiolate anions. Interestingly, and given the lipophilic nature of **AcroB**, this indicates that reactions are occurring within the inner leaflet of the inner mitochondrial membrane. Consistent with this, a cross-section analysis of the mitochondria (Figure S5) shows that the majority of events occur at the center of a mitochondrion, highlighting the power of NASCA super-resolution imaging in deciphering the site of reaction.

In addition to rendering spatial information, single-molecule analysis of fluorescence bursts enabled counting chemical events to determine the frequency of reactions between **AcroB** and the cellular proteome in a given cellular region. Figure 2A shows the number of adducts formed in different regions of the cell. Effectively, the number of unequivocally determined fluorescence bursts is from the two-dimensional image projection of the cell. A region of interest (ROI) of 1.66 μm in width and 250 nm in height was selected to count events detected in 500 frames (25 s) either in sections of mitochondria (200 to 300 events) sections of cell nucleus (<10 events), cellular regions with no apparent organelle (0 to 30 events), and extracellular regions (mostly no events). A total of 260000 events were detected in 500 frames (25 s) over the whole image shown in Figure 2A, that is ∼10000 events/s. These events were detected following excitation with the evanescent beam which interrogates the basal region of the cell.

Consistent with the activity in HeLa cells, results in a different cell line were comparable. Thus, the chemical activity of **AcroB** in MRC5 (ATCC CCL-171) lung fibroblast cells (Figure 3) showed events occurring predominately in mitochondria. Further, no significant difference was recorded in the frequency of events within mitochondria of the MRC5 cells compared to the HeLa cells for the same ROI. However, and given the lesser number and smaller size of the mitochondria of the MRC5 cells, we observed fewer chemical events overall for the whole cell.

AcroB thus reports the spatiotemporal coordinates of protein alkylation and the amount of adduct formation taking place per unit time.

Trafficking Visualized via Colocalization Imaging. In order to follow the fate of **AcroB** adducts formed within mitochondria, we next conducted imaging experiments reducing the excitation power ca. 5 orders of magnitude (to 0.002 mW). These conditions minimized the photobleaching of the newly formed fluorescent adducts, thus revealing where they accumulated rather than where they formed (Figure 4).

Intriguingly, studies at this low excitation power showed no accumulation of **AcroB** adducts within mitochondria in HeLa cells transiently expressing a red fluorescent marker of mitochondria (see Figure 4B and accompanying supplementary Video S4), albeit major accumulation was observed elsewhere in the cell (Figure 4 and discussion below). This result highlights that mitochondria are the source but not a sink of newly formed adducts. Importantly, we observed a number of vesicles containing **AcroB** adducts that appeared to pause trafficking when near a mitochondrion (Figure 4B, red arrows). We hypothesize that these are "kiss-and-run" fusion events[29] and merit further investigation.

We argue that newly formed **AcroB** adducts recruit/exploit a constitutive excretion mechanism within healthy mitochondria

DOI: 10.1021/jacs.7b08615
J. Am. Chem. Soc. 2017, 139, 16273−16281

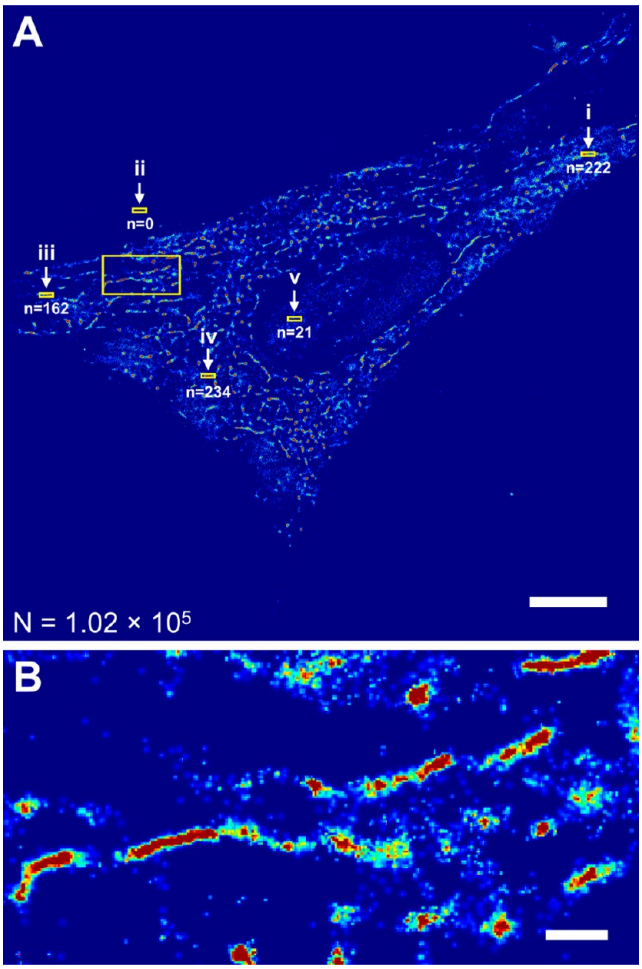

Figure 3. (A) NASCA high-resolution map of individual PTM events in an MRC5 cell accumulated over 500 consecutive frames (25 s) following treatment with 100 nM **AcroB**. *N* is the total number of observed chemical events. Events were counted if their intensity was greater than 1000 photons and less than 20000 photons. *n* is the number of chemical events counted in 1.66 μm × 250 nm regions within regions of interest corresponding to mitochondria (i,iii,iv), the nucleus (v), and extracellular region (ii) are listed. Scale bar is 10 μm. (B) Magnified region showing **AcroB** adduct hot-spots corresponding to mitochondria. Scale bar is 1 μm.

that ensures rapid disposal of compromised proteins. The inner mitochondrial membrane is particularly susceptible to lipid peroxidation and subsequent LDE formation, given the generation of reactive oxygen species formed as byproducts of the electron transport chain. It is thus highly plausible that **AcroB** is effectively illuminating the dynamics of detoxification of electrophiles to mitigate damage associated with metabolic activity.

To map the sorting, trafficking, and segregation of protein−**AcroB** adducts within the cell following their generation in mitochondria,[30] HeLa cells were next costained or transfected with markers for structural compartments within the endomembrane system including Golgi apparatus, early endosomes and lysosomes, and with markers for microtubules (Figure 4) and imaged at low excitation powers (0.06 mW). Pulse-chase imaging experiments on cells transiently expressing a red emissive marker of the Golgi apparatus illustrated the accumulation of fluorescent adducts was predominantly observed within this membrane rich organelle immediately following addition of **AcroB** (Figure 4C and Video S5). Concomitant with this initial increase in fluorescence in the Golgi apparatus, we observed the prominent and conspicuous translocation of carriers/vesicular bodies, a few hundreds of nanometers in diameter, transporting accumulated **AcroB**−protein adducts along a directional pattern (both inward and outward of the cell) within the cytosol. These dynamics are consistent with transport along microtubules.[31] Colocalization studies with tubulin-RFP confirmed the assignment (Figure 4D and Video S6).

Following the transport along microtubules and initial Golgi accumulation, fluorescence images also exhibited, within minutes of adding **AcroB**, a number of branched, tubular structures which were consistent in profile to fluorescence[32] and electron microscopy images of early endosomes.[33] To confirm the assignment, we conducted two-color imaging experiments with HeLa cells transiently expressing red fluorescent protein (RFP) fused to Rab5a, a protein recruited in early endosomes.[30] These experiments enabled visualizing the transfer of **AcroB**−protein adducts within carriers into RFP-tagged early endosomes near the cell periphery manifested as a colocalization of green and red stained organelles (Figure 4E,F). We were next able to follow the progression of early endosomes toward the cell nucleus (Videos S7 and S8).

Our imaging experiments additionally enabled us to record the sorting of **AcroB**−protein adducts within the endocytic pathway. Figure 4F displays the extension of a lipid tubule originating from a concentrated pocket of **AcroB** adducts that upon extrusion—presumably along a microtubule as may be judged from its straight linear morphology—and fission releases carriers that fuse next with nearby early endosomes. We also recorded lipid tubular structures containing **AcroB** adducts that extruded extending all the way to the cell periphery where loss of fluorescence occurred (Figure 4E, white arrow). We speculate that the latter process marks the exocytosis of **AcroB**−protein adducts. In all cases, lipid tubular structures appeared to extrude and extend along a template,[34] which we assign to microtubules. Colocalization of **AcroB**−protein adducts with lysosomes was also observed, albeit taking place only after 30 min following the addition of **AcroB**, in two-color imaging studies conducted with LysoTracker Deep Red (Figure 4G and Video S9). This would indicate that adducts may also be sorted from late endosomes into lysosomes for recycling.

In contrast to the above, MRC5 cells (Figure 5) show significantly less accumulation of fluorescence products compared to HeLa cells after identical treatment. The lower number of products is consistent with results observed during NASCA imaging and the fewer adducts formed overall within the MRC5 cells (see above).

Control experiments at low excitation power (0.002 mW) with an emissive BODIPY dye bearing a saturated aldehyde at the *meso*-position (compound **5**) as well as with the BODIPY reporter used in **AcroB** (**H_2BEt**)[14] were conducted to monitor the distribution of BODIPY to rule out that the associated reactivity is the outcome of preferential mitochondrial membrane partitioning over other membrane environments. Both control fluorophores stained the various membranes of the cell, with slightly higher intensity in the membrane-rich mitochondria (Figure S6). Under the same experimental conditions, **AcroB**-alkylated products were observed to accumulate elsewhere but in mitochondria (nonreacted **AcroB** would not be observed at all). Altogether the results

DOI: 10.1021/jacs.7b08615
J. Am. Chem. Soc. 2017, 139, 16273−16281

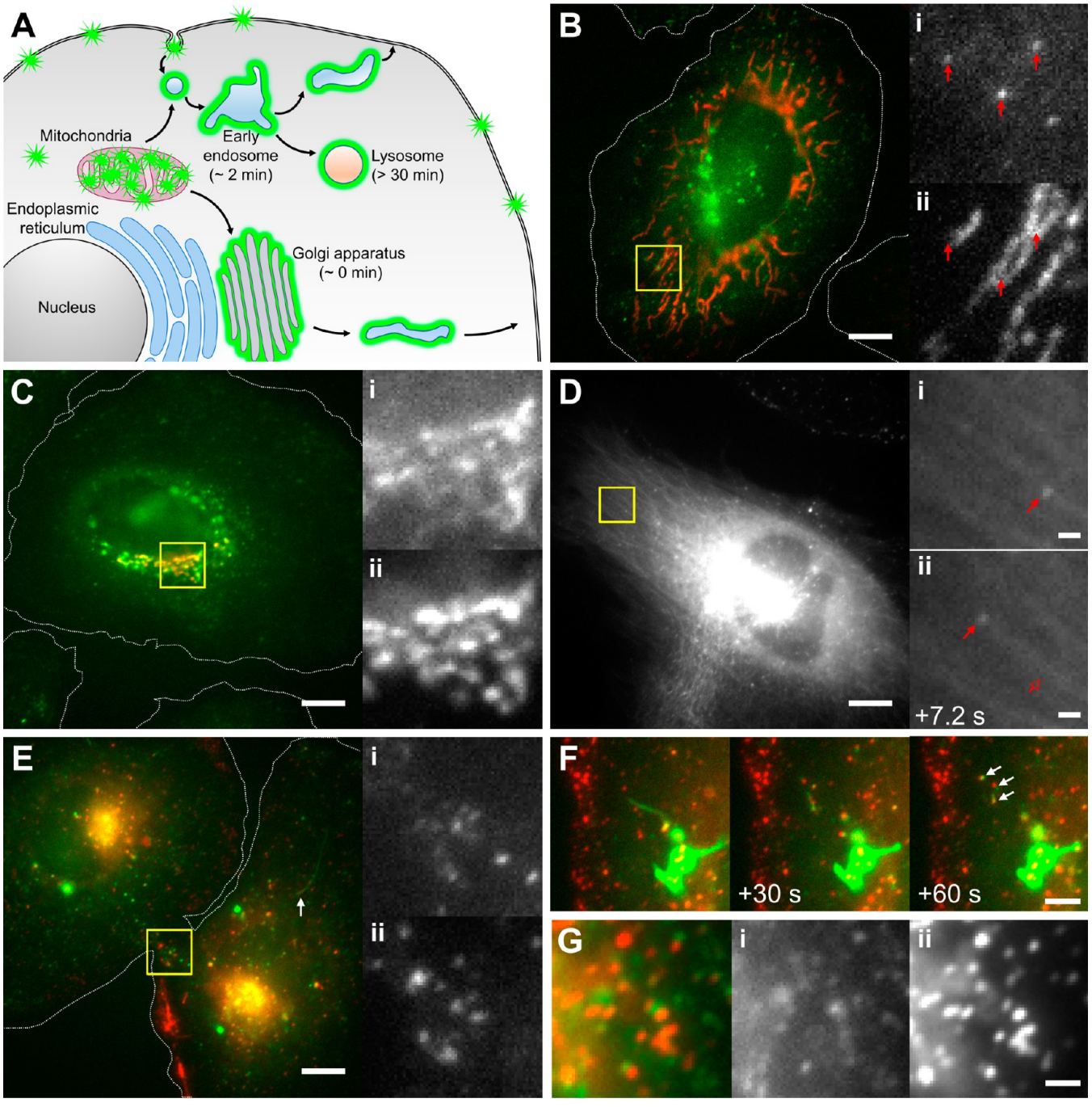

Figure 4. (A) Schematic representation of the generation and subsequent trafficking and accumulation of **AcroB** fluorescent products along various cell organelles. (B) TIRF microscopy of a cell transiently expressing CellLight mitochondria-RFP (red) treated with **AcroB** (green). (i) **AcroB** fluorescence only. (ii) RFP fluorescence only. Red arrows denote mitochondria-associated vesicles. (C) Wide-field fluorescence microscopy of a cell transiently expressing CellLight Golgi-RFP (red) treated with **AcroB** (green). (i) **AcroB** fluorescence only. (ii) RFP fluorescence only. (D) TIRF microscopy of a cell transiently expressing CellLight Tubulin-RFP treated with **AcroB**. The movement of a vesicle (red arrow) can be followed along a microtubule (i) at time 0 and (ii) 7.2 s later. Scale bars are 1 μm. (E) Wide-field fluorescence microscopy of a cell transiently expressing CellLight Early Endosome-RFP (red) treated with **AcroB** (green). The white arrow denotes a vesicle extrusion bearing **AcroB** adducts toward the cell periphery. (i) **AcroB** fluorescence only. (ii) RFP fluorescence only. (F) Wide-field fluorescence microscopy of a cell transiently expressing CellLight Early Endosome-RFP (red) treated with **AcroB** (green) showing extrusion and sorting of **AcroB** adducts into early endosomes denoted with white arrows. (G) Wide-field fluorescence microscopy of a cell costrained with **AcroB** (green) and LysoTracker Deep Red (red) 30 min after addition of **AcroB**. (i) **AcroB** fluorescence only. (ii) LysoTracker fluorescence only. Scale bars are 10 μm except (F,G) at 5 and 2 μm, respectively. Zoomed-in regions are 10 × 10 μm but in (D).

highlight that the localization of the BODIPY compounds lies within lipid membranes with no specific organelle targeting and that the chromophore trafficking is very different for **AcroB** adducts versus fluorescent control compounds.

Control compound **5** and the parent chromophore **H_2BEt** provided an additional advantage, namely, to factor out whether the frequency of events observed at high excitation powers depends on the local probe concentration, the cysteine-

DOI: 10.1021/jacs.7b08615
J. Am. Chem. Soc. 2017, 139, 16273−16281

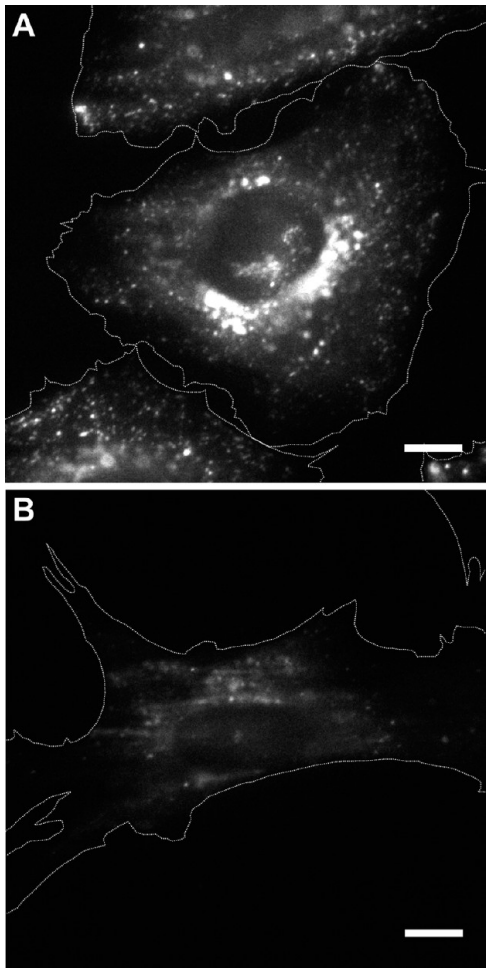

Figure 5. TIRF microscopy of HeLa (A) and MRC5 (B) cells 15 min following treatment with **AcroB**, showing significantly more fluorescent products accumulated in the HeLa cell. Cell perimeters are delineated with a white line. Scale bars are 10 μm.

containing protein/peptide concentration, or the activity of both. Both compounds, being intrinsically fluorescent, enabled recording the arrival time of dyes/replenishing under conditions of high excitation power (42 mW) established with the evanescent field in our TIRF setup, analogous to PAINT method.[35] Here a steady-state condition will be established where newly arrived fluorophores will be rapidly photobleached. Counting events under this steady-state condition and comparing these to the steady-state condition recorded with **AcroB** alkylation yielded similar event counts indicating that the rate limiting step is the arrival of the BODIPY chromophore (Figure S6).

Isolation of AcroB Adducts. In order to shed light on molecular targets of **AcroB**, we conducted SDS-PAGE studies on extracts of HeLa cells that had been incubated for 30 min in the presence of 50 μM of the **AcroB** warhead (see Figure 6 and also Supporting Information for details). We note that the much higher concentrations utilized herein are in line with those reported in cellular proteomic studies of nonenal.[5,11,36,37] Given the predominance of **AcroB** adducts observed in mitochondria and endocytic pathway, we elected to utilize differential centrifugation to fraction the cell extract. Cells were lysed by passing through a 26 gauge needle. A low-speed centrifugation was used to remove the nuclei, debris, and any

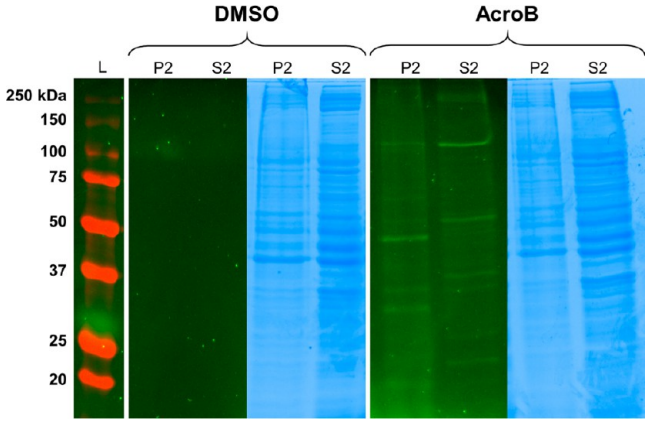

Figure 6. SDS-PAGE of **AcroB** protein adducts from HeLa cell fractions. Cells were treated with DMSO or **AcroB**, and various cellular components were extracted by differential centrifugation. Both fluorescence (**AcroB** and **Cy5**, green and red, respectively) and Coomassie stained (blue) lanes are shown. Green fluorescence shows discrete bands from fractions P2 (mitochondria, endosomes) and S2 (cytosolic proteins) of cells treated with **AcroB** compared to no fluorescence in controls with DMSO.

intact cells (P1). The resulting supernatant (S1) was spun at a higher speed to deposit mitochondria, endosomes, and lysosomes (P2), with cytosolic components and smaller lipid fragments in the supernatant (S2).[38] See Figure S7 for the full gels imaged in both fluorescence and following staining with Coomassie Blue.

A number of fluorescent bands over a large range of molecular weights were recorded when imaging the gel for **AcroB** emission. Several fluorescent bands correlated in intensity with Coomassie staining, yet fluorescence also aligned in regions barely stained by Coomassie, illustrating the potential for **AcroB** to mark nonprevalent protein targets. This property is the result of its high emission enhancement upon protein alkylation, demonstrating its potential as a reporter for product studies. Future proteomic studies will reveal the chemical nature of the adducts in these bands. Of note, a major band overpowering those displayed in the gel was observed with the loading-dye front. The product may be assigned to alkylation of low molecular weight thiols, in particular, glutathione, which we argue may take place, catalyzed by membrane-associated GST found within mitochondria.[39]

■ CONCLUSION

Combining a reactive electrophile with a fluorescence reporter, an approach to study the effects of electrophile alkylation on living cells has been developed. The fluorogenic probe **AcroB** can be used toward mapping chemical reactions within the cell lipid milieu, in particular, mitochondria, with super-resolution accuracy as well as toward revealing the complex system of recycling mechanisms and its dynamics necessary for a cell to sort and process electrophile adducts. **AcroB** may thus help elucidate key aspects of mitochondria electrophile adduct excretion and cell endocytic and exocytic pathways. It may also help illustrate key mechanisms involved in sorting and clearance, their consequences for physiology and pathology, notably in healthy versus sick cells. The studies may be carried out at low electrophile concentrations analogous to those of endogenous electrophiles such as 4-HNE.

DOI: 10.1021/jacs.7b08615
J. Am. Chem. Soc. 2017, 139, 16273−16281

By counting individual chemical events (fluorescence bursts), positioning them in place (tens of nm) and time (ms), information on the dose and spatiotemporal requisites to induce a response may be retrieved. We believe the new methodology for probing the spatiotemporal response of the cell milieu to electrophiles will be important in understanding neurodegenerative diseases[40,41] and other pathologies resulting from oxidative stress and lipid autoxidation and the generation of LDEs.

At the imaging level, our approach is one where we "probe the probe". Essentially, the new fluorogenic acrolein−BODIPY is conceived as an active chemical player that, provided with a warhead, can only be traced once it has yielded the desired chemical product. Here, the outcome of the reaction is a flare or fluorescence burst that can be imaged one at a time. We have thus provided a new paradigm in fluorescence imaging. That is, while fluorescent probes up to now have been utilized either as positional tags, or to report on conformation fluctuations via FRET, or to sense their chemical environment, the fluorogenic acrolein warhead actively perturbs the system simultaneously reporting its chemical transformation.

■ ASSOCIATED CONTENT

Supporting Information

The Supporting Information is available free of charge on the ACS Publications website at DOI: 10.1021/jacs.7b08615.

Materials and methods, including synthesis of AcroB and its precursors; methodologies for microscopy, computational studies, liposome assays, partition coefficient determination, cell culture and staining, SDS-PAGE, and image analysis; supplemental figures and video descriptions; ^{1}H NMR and ^{13}C NMR spectra of AcroB and its precursors (PDF)

Video S1 (MP4)
Video S2 (MP4)
Video S3 (MP4)
Video S4 (MP4)
Video S5 (MP4)
Video S6 (MP4)
Video S7 (MP4)
Video S8 (MP4)
Video S9 (MP4)

■ AUTHOR INFORMATION

Corresponding Author

*gonzalo.cosa@mcgill.ca

ORCID

Gonzalo Cosa: 0000-0003-0064-1345

Notes

The authors declare no competing financial interest.

■ ACKNOWLEDGMENTS

G.C. is grateful to the Natural Sciences and Engineering Research Council (NSERC) of Canada and the Canadian Foundation for Innovation (CFI) for funding. R.L. is thankful to NSERC for a postgraduate scholarship. L.E.G. is thankful to Vanier Canada for a postgraduate scholarship. W.Z. is thankful to NSERC for a postgraduate scholarship.

■ REFERENCES

(1) Yin, H.; Xu, L.; Porter, N. A. *Chem. Rev.* **2011**, *111* (10), 5944−72.

(2) Halliwell, B.; Gutteridge, J. M. C. *Free Radicals in Biology and Medicine*, 5th ed.; Oxford University Press: Oxford, 2015.

(3) Perluigi, M.; Coccia, R.; Butterfield, D. A. *Antioxid. Redox Signaling* **2012**, *17* (11), 1590−609.

(4) Beavers, W. N.; Rose, K. L.; Galligan, J. J.; Mitchener, M. M.; Rouzer, C. A.; Tallman, K. A.; Lamberson, C. R.; Wang, X.; Hill, S.; Ivanova, P. T.; Brown, H. A.; Zhang, B.; Porter, N. A.; Marnett, L. J. *ACS Chem. Biol.* **2017**, *12*, 2062.

(5) Yang, J.; Tallman, K. A.; Porter, N. A.; Liebler, D. C. *Anal. Chem.* **2015**, *87* (5), 2535−41.

(6) Shibata, T.; Shimozu, Y.; Wakita, C.; Shibata, N.; Kobayashi, M.; Machida, S.; Kato, R.; Itabe, H.; Zhu, X.; Sayre, L. M.; Uchida, K. *J. Biol. Chem.* **2011**, *286* (22), 19943−19957.

(7) Rudolph, T. K.; Freeman, B. A. *Sci. Signaling* **2009**, *2* (90), re7.

(8) Lin, H. Y.; Haegele, J. A.; Disare, M. T.; Lin, Q.; Aye, Y. *J. Am. Chem. Soc.* **2015**, *137* (19), 6232−44.

(9) Galligan, J. J.; Rose, K. L.; Beavers, W. N.; Hill, S.; Tallman, K. A.; Tansey, W. P.; Marnett, L. J. *J. Am. Chem. Soc.* **2014**, *136* (34), 11864−6.

(10) Crunkhorn, S. *Nat. Rev. Drug Discovery* **2012**, *11* (2), 96.

(11) Zhang, H.; Forman, H. J. *Arch. Biochem. Biophys.* **2017**, *617*, 145−154.

(12) Wang, C.; Weerapana, E.; Blewett, M. M.; Cravatt, B. F. *Nat. Methods* **2013**, *11* (1), 79−85.

(13) Krumova, K.; Cosa, G. *J. Am. Chem. Soc.* **2010**, *132* (49), 17560−9.

(14) Lincoln, R.; Greene, L. E.; Bain, C.; Flores-Rizo, J. O.; Bohle, D. S.; Cosa, G. *J. Phys. Chem. B* **2015**, *119* (13), 4758−65.

(15) Loudet, A.; Burgess, K. *Chem. Rev.* **2007**, *107* (11), 4891−932.

(16) Godin, R.; Liu, H. W.; Smith, L.; Cosa, G. *Langmuir* **2014**, *30* (37), 11138−46.

(17) Krumova, K.; Greene, L. E.; Cosa, G. *J. Am. Chem. Soc.* **2013**, *135* (45), 17135−43.

(18) Frisch, M. J.; Trucks, G. W.; Schlegel, H. B.; Scuseria, G. E.; Robb, M. A.; Cheeseman, J. R.; Scalmani, G.; Barone, V.; Petersson, G. A.; Nakatsuji, H.; Li, X.; Caricato, M.; Marenich, A. V.; Bloino, J.; Janesko, B. G.; Gomperts, R.; Mennucci, B.; Hratchian, H. P.; Ortiz, J. V.; Izmaylov, A. F.; Sonnenberg, J. L.; Williams-Young, D.; Ding, F.; Lipparini, F.; Egidi, F.; Goings, J.; Peng, B.; Petrone, A.; Henderson, T.; Ranasinghe, D.; Zakrzewski, V. G.; Gao, J.; Rega, N.; Zheng, G.; Liang, W.; Hada, M.; Ehara, M.; Toyota, K.; Fukuda, R.; Hasegawa, J.; Ishida, M.; Nakajima, T.; Honda, Y.; Kitao, O.; Nakai, H.; Vreven, T.; Throssell, K.; Montgomery, J. A., Jr.; Peralta, J. E.; Ogliaro, F.; Bearpark, M. J.; Heyd, J. J.; Brothers, E. N.; Kudin, K. N.; Staroverov, V. N.; Keith, T. A.; Kobayashi, R.; Normand, J.; Raghavachari, K.; Rendell, A. P.; Burant, J. C.; Iyengar, S. S.; Tomasi, J.; Cossi, M.; Millam, J. M.; Klene, M.; Adamo, C.; Cammi, R.; Ochterski, J. W.; Martin, R. L.; Morokuma, K.; Farkas, O.; Foresman, J. B.; Fox, D. J. *Gaussian 16*; Gaussian Inc.: Wallingford, CT, 2016.

(19) Koch, W.; Holthausen, M. C. *A Chemist's Guide to Density Functional Theory*; John Wiley & Sons: New York, 2015.

(20) Sangster, J. *J. Phys. Chem. Ref. Data* **1989**, *18* (3), 1111−1229.

(21) Romieu, A.; Massif, C.; Rihn, S.; Ulrich, G.; Ziessel, R.; Renard, P.-Y. *New J. Chem.* **2013**, *37* (4), 1016−1027.

(22) Drummen, G. P. C.; van Liebergen, L. C. M.; Op den Kamp, J. A. F.; Post, J. A. *Free Radical Biol. Med.* **2002**, *33* (4), 473−490.

(23) Rust, M. J.; Bates, M.; Zhuang, X. *Nat. Methods* **2006**, *3* (10), 793−5.

(24) Betzig, E.; Patterson, G. H.; Sougrat, R.; Lindwasser, O. W.; Olenych, S.; Bonifacino, J. S.; Davidson, M. W.; Lippincott-Schwartz, J.; Hess, H. F. *Science* **2006**, *313* (5793), 1642−5.

(25) Hess, S. T.; Girirajan, T. P.; Mason, M. D. *Biophys. J.* **2006**, *91* (11), 4258−72.

(26) Roeffaers, M. B.; De Cremer, G.; Libeert, J.; Ameloot, R.; Dedecker, P.; Bons, A. J.; Buckins, M.; Martens, J. A.; Sels, B. F.; De Vos, D. E.; Hofkens, J. *Angew. Chem., Int. Ed.* **2009**, *48* (49), 9285−9289.

DOI: 10.1021/jacs.7b08615
J. Am. Chem. Soc. 2017, 139, 16273−16281

(27) Hurd, T. R.; Costa, N. J.; Dahm, C. C.; Beer, S. M.; Brown, S. E.; Filipovska, A.; Murphy, M. P. *Antioxid. Redox Signaling* **2005**, *7* (7−8), 999−1010.
(28) Schopfer, F. J.; Cipollina, C.; Freeman, B. A. *Chem. Rev.* **2011**, *111* (10), 5997−6021.
(29) Liu, X.; Weaver, D.; Shirihai, O.; Hajnoczky, G. *EMBO J.* **2009**, *28* (20), 3074−89.
(30) Grant, B. D.; Donaldson, J. G. *Nat. Rev. Mol. Cell Biol.* **2009**, *10* (9), 597−608.
(31) Bausinger, R.; von Gersdorff, K.; Braeckmans, K.; Ogris, M.; Wagner, E.; Brauchle, C.; Zumbusch, A. *Angew. Chem., Int. Ed.* **2006**, *45* (10), 1568−72.
(32) Li, D.; Shao, L.; Chen, B. C.; Zhang, X.; Zhang, M.; Moses, B.; Milkie, D. E.; Beach, J. R.; Hammer, J. A., 3rd; Pasham, M.; Kirchhausen, T.; Baird, M. A.; Davidson, M. W.; Xu, P.; Betzig, E. *Science* **2015**, *349* (6251), aab3500.
(33) Tooze, J.; Hollinshead, M. *J. Cell Biol.* **1992**, *118* (4), 813−830.
(34) De Matteis, M. A.; Luini, A. *Nat. Rev. Mol. Cell Biol.* **2008**, *9* (4), 273−84.
(35) Sharonov, A.; Hochstrasser, R. M. *Proc. Natl. Acad. Sci. U. S. A.* **2006**, *103* (50), 18911−18916.
(36) Vila, A.; Tallman, K. A.; Jacobs, A. T.; Liebler, D. C.; Porter, N. A.; Marnett, L. J. *Chem. Res. Toxicol.* **2008**, *21* (2), 432−44.
(37) Jacobs, A. T.; Marnett, L. J. *Acc. Chem. Res.* **2010**, *43* (5), 673−83.
(38) Lodish, H. F. *Molecular Cell Biology*, 4th ed.; W.H. Freeman: New York, 2000; p xxxvi, 1084, G-17, I-36 p.
(39) Raza, H.; Robin, M. A.; Fang, J. K.; Avadhani, N. G. *Biochem. J.* **2002**, *366*, 45−55.
(40) Li, X.; DiFiglia, M. *Prog. Neurobiol.* **2012**, *97* (2), 127−41.
(41) Halliwell, B. *J. Neurochem.* **2006**, *97* (6), 1634−58.

DOI: 10.1021/jacs.7b08615
J. Am. Chem. Soc. 2017, 139, 16273−16281